Optical Engineering, in press (1999)

Automatic enhancement of noisy image sequences through local spatio-temporal spectrum analysis

Oscar Nestares: Aerospace Division. SENER Ingeniería y Sistemas, S.A.
Severo Ochoa 4, 28760 Tres Cantos (Madrid). SPAIN
Phone: (34) 91 807 73 51 Fax: (34) 91 807 72 05
e-mail: oscar@optica.csic.es

Carlos Miravet: Aerospace Division. SENER Ingeniería y Sistemas, S.A.
Severo Ochoa 4, 28760 Tres Cantos (Madrid). SPAIN
Phone: (34) 91 807 73 56 Fax: (34) 91 807 72 05
e-mail: carlos.miravet@sener.es

Javier Santamaria: Aerospace Division. SENER Ingeniería y Sistemas, S.A.
Severo Ochoa 4, 28760 Tres Cantos (Madrid). SPAIN
Phone: (34) 91 807 73 50 Fax: (34) 91 807 72 05
e-mail: javier.santamaria@sener.es

Rafael Navarro: Instituto de Óptica "Daza de Valdés" (C.S.I.C.)
Serrano 121, 28006 Madrid. SPAIN
Phone: (34) 91 590 16 16 Fax: (34) 91 564 55 57
e-mail: r.navarro@fresno.csic.es

Abstract

A fully automatic method is proposed to produce an enhanced image from a very noisy sequence consisting of a translating object over a background with different translation motion. The method is based on averaging registered versions of the frames in which the object has been motion compensated. Conventional techniques for displacement estimation are not adequate for these very noise sequences, and thus a new strategy has been used taking advantage of the simple model of the sequences. First, the local spatio-temporal spectrum is estimated through a bank of multidirectional/multiscale third order Gaussian derivative filters, yielding a representation of the sequence that facilitates further processing and analysis tasks. Then, energy-related measurements describing the local texture and motion are easily extracted from this representation. These descriptors are used to segment the sequence based on a local joint measure of motion and texture. Once the object of interest has been segmented, its velocity is estimated applying the gradient constraint to the output of a directional band-pass filter for all pixels belonging to the object. Velocity estimates are then used to compensate the motion prior to the average. The results obtained with real sequences of moving ships taken under very noisy conditions are highly satisfactory, demonstrating the robustness and usefulness of the proposed method.

Keywords: Image enhancement, noisy sequences, joint transforms, image segmentation, motion estimation

1 Introduction

Image sequences contain highly redundant temporal information that can be used for restoration, resolution improvement or enhancement of the scene. One particularly simple case is a sequence of a still scene taken under time-varying degradations, such as random turbulence or noisy conditions. The effects of turbulence[1] or noise[2,3] can be diminished by simply averaging several frames, which tends to cancel the random variations.

Most image sequences, however, contain some motion. This motion causes that different frames contain the same object of interest but shifted, and possibly, rotated and scaled, thus providing slightly different views of the object. This fact has been used to reduce aliasing and then to improve resolution[4,5,6], especially in sparse sampling arrays used in infrared imaging systems, in cases having a relatively small amount of noise. In general, motion prevents the direct temporal integration of the frames, and hence it is difficult to reduce high amounts of noise. In these cases, it is necessary to determine the motion of the object of interest to compensate for it, prior to integration.

Image motion or optical flow estimation is an ill-posed problem[7], usually giving noisy results even in noise free sequences[8]. Last results suggest that an optimal strategy is to simultaneously estimate motion and segment the sequence, based on motion contents[9,10]. This strategy is more robust than a direct estimation of optical flow. These methods usually segment the sequence based on motion and compute optical flow iteratively (using algortihms like Expectation/Maximization), each step refining the previous one[11]. They have been successfully tested in complex sequences that include rotations and scaling, but that are free of noise. They are also computational expensive, since the convergence rates are usually slow. Other methods have been proposed for the simultaneous estimation of multiple optical flow present in the same spatial location[12], which are optimal when the sequence can be locally expressed as the linear superposition of several motion signals (e.g., additive transparency). This is not the case of our image sequences (as explained below), because there are not multiple motions at the same spatial location except at the occlusion boundaries, where the signal is not simply described as the linear superposition of several motion signals.

In this paper we have considered the case of sequences containing an object of interest undergoing a translation motion against a background undergoing a different translation motion, and with a very low signal to noise ratio due to the poor imaging conditions. The absence of relevant rotations or scaling of the target allows applying more robust methods than in the general case. This type of sequences is of great interest in certain applications, like ground-based maritime surveillance systems.

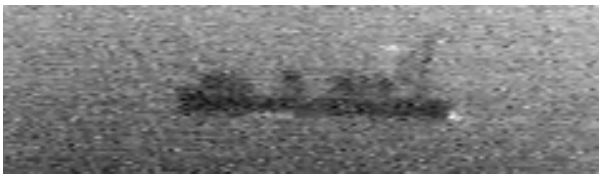

Figure 1. Sample frame of a typical sequence that has been taken from a static CCD camera within the range of visible, and that corresponds to a ship translating to the left.

The method applied for image enhancement is based on a visual representation of the image sequence that provides an estimate of the local spatio-temporal spectrum[13]. This generic scheme of representation was previously developed as a first multipurpose stage of sequence processing that is inspired in human vision and that facilitates further analysis and processing applications**.** In particular, it helps to segment, robustly, very noisy sequences based on texture and motion contents, a task where our visual system shows a high performance. After segmenting the moving object, we estimate its velocity by applying a modified version of a method for optical flow estimation based in the same representation of the image sequence, therefore requiring little additional cost[13]. The estimated velocity is then used to register the object in all frames, which are finally integrated to improve the signal-to-noise ratio.

We have tested the performance of each step of the method with synthetic test sequences contaminated with spatio-temporal noise of the same power than the original sequence (signal to noise ratio of 0dB). The method is able to detect and segment the moving object, and to estimate its velocity reliably. It was also tested with real sequences acquired from maritime surveillance (infrared and visible) imaging systems. The results show a remarkable enhancement in all cases.

2 Method

The method for image sequences enhancement has been developed for a particular class of sequences that consist of an object of interest moving against a background, and contaminated with spatio-temporal noise, so that the visibility of the target is very low. Concretely, these are the main assumptions about the sequences for which this method is applicable:

1. There is one object of interest, or target, which is undergoing a smooth translation motion, i.e., the image velocity of all the points belonging to the object is the same at a particular time (i.e., there are not noticeable rotations or scaling), and it varies slowly in time.
2. The object is against a background that is also undergoing a smooth translation motion, different from the motion of the target. We consider a static background as a particular case of zero velocity.

3. The resulting sequence is contaminated with white spatio-temporal noise of high power (in extreme cases, the same power than the signal).

Figure 1 shows a frame of a typical sequence that consists of a ship translating from right to the left, and that has been taken with a visible CCD camera under noisy conditions. The ship is both blurred and highly corrupted by noise, making its recognition difficult.

The proposed method obtains an enhanced version of the object of interest automatically, following these steps: (1) segmenting the object of interest; (2) estimating the velocity of the object and hence the displacements between frames; and (3) averaging motion compensated versions of the frames together.

The high level of noise present in our sequences makes the two first steps critical and especially difficult, requiring highly robust methods. Therefore, we have avoided using standard techniques relying on the analysis of static frames only (like segmentation by thresholding, or displacement estimation by correlation or block matching). Instead, the proposed method uses local spatio-temporal frequency information at each point in the sequence. The main stages of the method, displayed in the block diagram of Figure 2, are the following:

1. The local spatio-temporal spectrum of the sequence is estimated through a bank of band-pass, multidirectional/multiscale spatio-temporal filters. This produces a visual representation of the image sequence[13] that facilitates further analysis tasks.

2. The target is segmented from the background, using spatio-temporal descriptors derived from the above visual representation of the sequence[14]. These descriptors are defined at each point as local measurements of the energy at each specific frequency band, and hence of the texture-motion energy at each location[15]. These descriptors are an extension of those used previously in multichannel static texture segmentation[16,17,18,19]. In this dynamic case, differences in velocity, texture or both, are the key features to discriminate the target from the background.

3. The target's velocity is estimated for each frame, to compute its displacements and to register it in the different frames. Velocity is estimated using a modified version of a previously developed method for probabilistic multichannel optical flow estimation[13]. Optical flow is estimated applying the gradient constraint[20] to the output of a directional band-pass filter, chosen to respond mainly to the moving object, thus eliminating a great amount of noise. In addition, since the prior segmentation has already detected the points of the target, which share the same velocity, combining gradient constraints in this relatively high number of points, strongly improves robustness and accuracy of the velocity estimate.

4. The motion is compensated for every image so that the object appears registered, making possible the final integration of all frames to give a single enhanced image of the object of interest.

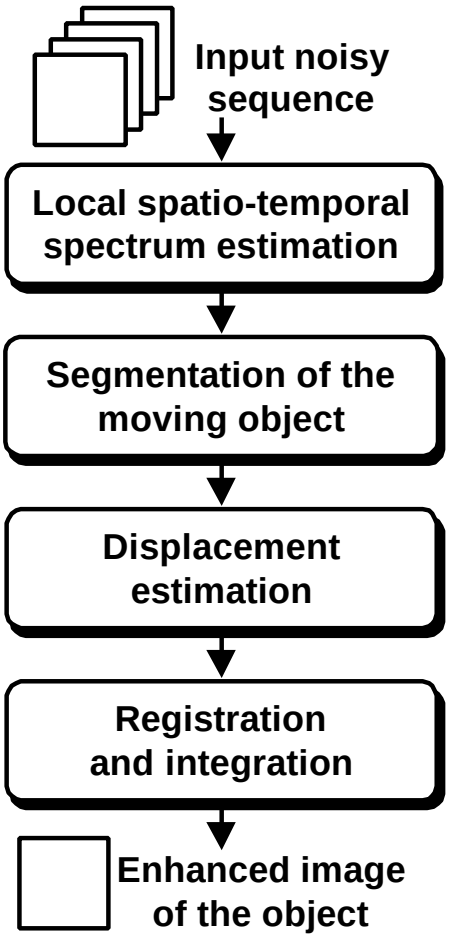

Figure 2. Block diagram of the proposed method for image enhancement from noisy sequences.

We give a detailed explanation of these stages in the next paragraphs. To test and optimize these stages, we have generated synthetic test sequences imitating real ones, but that constitute an extreme case where the only cue to segment the object is motion. The patterns used for the object and the background, displayed in Figure 3a and 3b respectively, are different samples of the same spatial fractal noise with power spectra proportional to $1/f_s^2$, where f_s is the radial spatial frequency. An ensemble of test sequences has been generated translating the object and the background with different velocities, and adding different amounts of spatio-temporal Gaussian white noise (Figure 3c). A frame of one of the resulting sequences (with SNR = 0 dB) is shown in Figure 3d, where the object is invisible

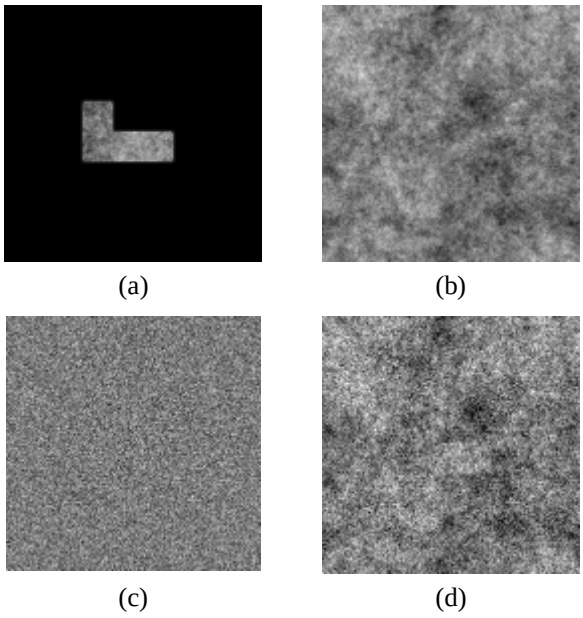

Figure 3. Generation of synthetic test sequences: (a) moving object filled with a synthetic fractal noise texture; (b) background consisting of a different sample of the same fractal noise; (c) additive spatio-temporal Gaussian white noise; (d) resulting frame.

to the eye. The object becomes clearly perceptible, however, when the sequence is displayed in motion.

2.1 *Local spectrum estimation*

The local spectrum has been estimated using a bank of multidirectional/multiscale band-pass spatio-temporal linear filters. For this purpose we have applied a previously developed scheme for visual representation of image sequences that has been designed as a multipurpose preprocessing stage to facilitate many image sequence processing and analysis applications[13].

The basis functions of this scheme are spatio-temporal third order Gaussian derivatives along specified spatio-temporal directions (GD3). Gaussian derivatives had been used by different authors[21,22] to model the early linear stages of the visual system. These filters have their tuning (peak) frequencies placed over the surface of a sphere (more generally, over an ellipsoid) for a given scale. The basis functions can be expressed as linear combinations of the separable functions obtained by third order (partial) derivation of a spatio-temporal Gaussian. The general expression, in the spatio-temporal frequency domain, for the separable basis (GD3) is the following:

$$\frac{\partial^3 g(x,y,t)}{\partial x^{3-k-l}\partial y^k \partial t^l} \quad \stackrel{F}{\longleftrightarrow} \quad (j2\pi f_x)^{3-k-l}(j2\pi f_y)^k (j2\pi f_t)^l G(f_x)G(f_y)G(f_t) \tag{1}$$

Table 1. Spherical angular coordinates of the directions where the 10 directional GD3 are placed at a each scale.

q	0	$\frac{\pi}{4}$	$\frac{\pi}{2}$	$\frac{3\pi}{2}$	0	$\frac{2\pi}{5}$	$\frac{4\pi}{5}$	$\frac{6\pi}{5}$	$\frac{8\pi}{5}$	-
j	$\frac{\pi}{2}$				asin($\frac{5}{8}$)					0

where $\stackrel{F}{\longleftrightarrow}$ means Fourier transform, (f_x, f_y, f_t) are the frequencies along the (two) spatial and the temporal axes, and $g(x)$ (with Fourier transform $G(f_x)$) is the following basic 1D Gaussian function:

$$g(x) = \frac{1}{\sqrt{2\pi}\sigma}\exp\left(-\frac{x^2}{2\sigma^2}\right) \stackrel{F}{\longleftrightarrow} G(f_x) = \exp\left(-\frac{\sigma^2}{2}(2\pi f_x)^2\right) \tag{2}$$

There are 10 independent GD3s at each scale, that correspond to all possible combination of indexes $0 \le l \le 3$ and $0 \le k \le 3-l$. A very efficient implementation using 1D convolution masks is possible, since the set of partial derivatives is separable. The directional filters, needed to obtain good samples of the local spectrum, are easily obtained from the set of partial derivatives through linear combination, a general property of directional derivatives closely related with the steerability of derivative filters [23,24]:

$$\frac{\partial^3 g(x,y,t)}{\partial \vec{h}_0^3} = \sum_{l=0}^{3}\sum_{k=0}^{3-l}\binom{3}{l}\binom{3-l}{k} \cos^{N-l-k}\theta_0 \sin^k\theta_0 \sin^{N-l}\phi_0 \cos^l\phi_0 \frac{\partial^3 g(x,y,t)}{\partial x^{3-k-l}\partial y^k \partial t^l} \tag{3}$$

where $\vec{h}_0$ is the spatio-temporal direction of derivation, which is determined by its spherical angular coordinates (θ_0, ϕ_0).

Table 1 contains the spherical angular coordinates of the 10 directions in the frequency domain that we have chosen to place the directional GD3 channels, at each scale. Four channels are placed in the static plane, defined by $f_t = 0$, all their centers (tuning frequencies) having $\phi = \pi/2$ in spherical coordinates, and equally spaced in azimuth. Five channels are placed in a dynamic plane parallel to the static plane. If we want to maintain the same amount of overlap in azimuth for these 5 dynamic channels, as for the static ones, then it follows that $\theta = \text{asin}(5/8)$ for this dy-

Table 2. One-dimensional 9-tap convolution masks corresponding to the Gaussian prefilter (g_0) and their derivatives of first (g_1), second (g_2) and third order (g_3), and 5-tap cubic B-spline filter Only the positive axis coefficients are shown, since g_0, g_2 and the cubic B-Spline are even-symmetric, and g_1 and g_3 are odd-symmetric.

g_0	3.616e-1	2.400e-1	6.968e-2	9.066e-3	4.437e-4
g_1	0	-2.072e-1	-1.203e-1	-2.347e-2	-1.541e-3
g_2	-3.254e-1	-4.084e-2	1.468e-1	5.036e-2	6.428e-3
g_3	0	4.107e-1	-3.534e-2	-8.794e-2	-1.934e-2
CBS	0.375	0.25	0.0625	-	-

namic plane[1]. The remaining 10th channel is placed on the pure temporal frequency axis.

The highest frequency scale has been placed at a radial tuning frequency of half the Nyquist frequency (1/4 cycles/sample). The GD3 filters have been implemented efficiently using the 1D small (9-tap) convolution masks shown in Table 2, obtaining high fidelity approximations of the theoretical frequency responses (greater than 30dB). Once the response to the separable (partial) derivative filters is obtained, it is straightforward to obtain the response to the directional ones, applying Eq. 3. Coarser scales have been obtained using an efficient pyramidal implementation, where the same set of filters corresponding to the finest scale is applied to successive subsampled versions (in space and time in a factor of 2) of the original sequence. The filter used to avoid aliasing in the subsampling operations is the 5-tap cubic B-Spline shown in Table 2. The resulting distribution of channels in the frequency domain is shown in Figure 4. This schematic view displays one slice along the one spatial frequency axis (f_x) and the temporal frequency axis (f_t). Channels corresponding to three spatio-temporal scales are represented by level curves of uniform magnitude response.

This implementation introduces a delay of 4 frames for the highest resolution level. The delay is multiplied by 2 as we move to coarse resolution levels. If the delay for coarser scales becomes critical for some applications, it is possible to use a version of the filter bank that uses multiresolution only in space[13], so that the maximum temporal delay is always of 4 frames. The main disadvantage of this version is that the samples of the spatio-temporal frequency domain are not evenly distributed.

[1] Each channel has two lobes, but whereas the 4 static channels yield a total of 8 lobes in one single static plane, dynamic channels produce 5 lobes in the positive dynamic plane, and other 5 lobes in another negative plane placed symmetrically with respect to the origin.

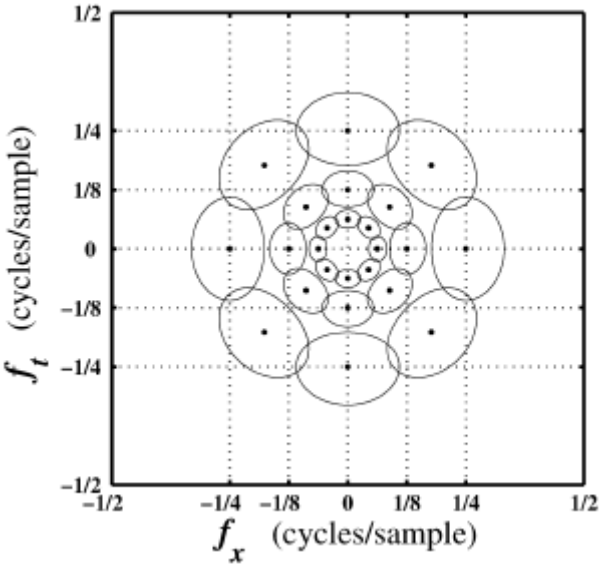

Figure 4. Schematic view of the directional GD3 channels, as a contour level plot, in a slice of the 3D spatio-temporal Fourier space corresponding to (f_x, f_t).

2.2 *Segmentation*

The target is segmented by unsupervised pixel classification, consisting of an automatic grouping of the pixels corresponding to the moving object. This process requires a local description of specific features that serve to discriminate between object and background. One such feature is precisely motion, since object and background display different motions in the sequences of interest.

Motion can be described taking into account the special form that takes the spatio-temporal spectrum of a given pattern undergoing uniform translation. It is well known that this spectrum is confined to a plane, whose azimuth and elevation depend on the orientation and modulus of the velocity, respectively[25]. More precisely, this plane is given by:

$$f_x v_x + f_y v_y + f_t = 0 \qquad (4)$$

where (f_x, f_y, f_t) are the components of the spatio-temporal frequency vector, and (v_x, v_y) the components of the velocity vector, respectively. The spatio-temporal spectrum of such a moving pattern is formed by the projection, parallel to the temporal frequency axis, of the 2D spatial spectrum of the spatial pattern (which is contained in the static plane given by $f_t = 0$), onto the plane given by Equation 4. Patterns undergoing different motions will have their spectra in separated planes. Thus, each pixel in the sequence can be characterized using measurements of the local energy of the spatio-temporal spectrum (joint texture-motion descriptors). The local spatio-temporal

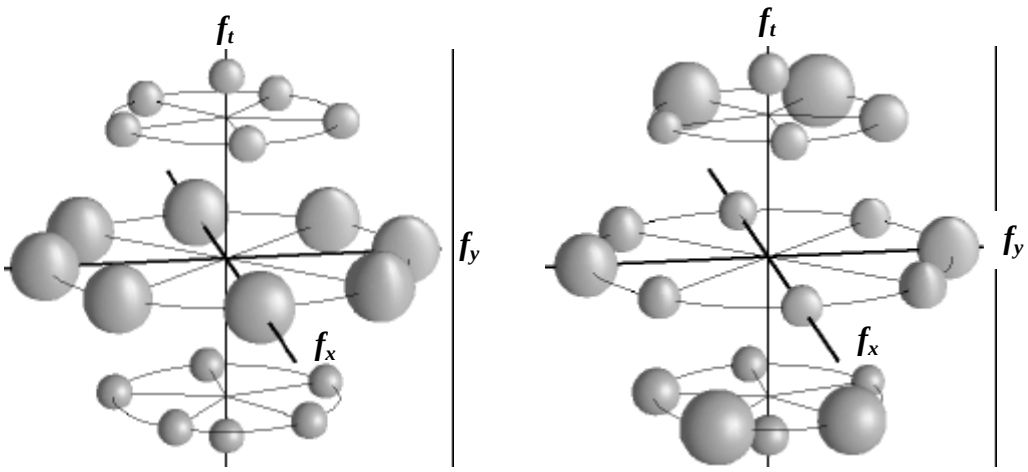

(a) (b)

Figure 5. Schematic view of the average energy of the finest scale channels, for the two regions: (a) background; and (b) moving object, of the synthetic test sequence of Figure 3. Each channel is represented by a pair of spheres centered at its tuning frequency, whose radius is proportional to the average energy inside the corresponding region.

spectrum will be different for pixels belonging to regions undergoing different motions, or having different textures. Local spectrum descriptors can be directly obtained from the representation of the sequence described in Section 2.1.

2.2.1 *Local spectrum energy descriptors*

The GD3 filter bank is sampling the local spectrum, but it is not convenient to use the direct output of the filters as descriptors, since these outputs depend on the local phase, and thus they are not shift-invariant. This problem is the same as in static texture discrimination, where it is usual to apply a non-linearity at the output of the filter bank[16,19,26] to obtain shift-invariant descriptors. Thus, we have extended a previous method for static texture segmentation[19] to the present problem of spatio-temporal segmentation. Results showed that the complex modulus produced better results than the energy and other tested non-linearities[27].

This can be implemented obtaining first complex samples of the local spectrum, using a pair of filters in phase quadrature, and then computing the modulus of these complex samples. However, to avoid designing and computing the responses to the quadrature pair corresponding to each GD3 filter, we have followed an approximate strategy that uses only the responses of the GD3 filters. The modulus of the complex samples obtained through a pair of quadrature filters is equivalent to the modulus of the response to one of the filters, previously shifted in the frequency domain such that their peak coincides with the zero frequency, and filtering with an appropriate ideal low-pass filter. In our case, since the GD3s filters are not perfect band-limited, and the ideal low-pass filter has been approximated using a spatio-temporal separable Cubic-B Spline filter (see Table 2), the result is not exactly the same than the modulus of the quadrature pair. Nevertheless, it is a very good approximation for our purposes.

Figure 5 illustrates how the signal (modulus) is distributed across the 10 channels of the highest frequency level, for the background (a) and the object (b) of the synthetic test sequence of Figure 3. Channel energy is represented by two opposite spheres centered at the channel's tuning frequency, and whose size is proportional to the average modulus of the channel response inside the corresponding region (background or object). The graph in panel (a) corresponds to the average energy distribution of each channel in the static background. In this case, the static channels are most excited (bigger spheres), but dynamic channels also display a moderate amount of energy, coming from the spatio-temporal additive white noise. The moving object (b) displays a clearly different distribution of energy. Here, most static channels are solely excited by the spatio-temporal white noise. In addition, two dynamic channels, which are close to the plane given by the translation velocity of the object, exhibit higher responses (bigger spheres), while those dynamic channels that are far away from that plane are not excited by the target but only by the white noise (smaller spheres). The approximately constant size of the smaller spheres in both cases is the result of the white noise.

These spatio-temporal spectral descriptors seem to be able to characterize, and hence to discriminate regions undergoing different translational motions, even under extremely noisy conditions, such as in the example shown here. Although Fig. 5 shows the average, over all pixels of the sequence belonging to the background (a) or target (b), it is worth noting that the descriptors are defined at each point, from a local spatio-temporal neighborhood, whose size is adapted to the frequency band according to the multiresolution scheme.

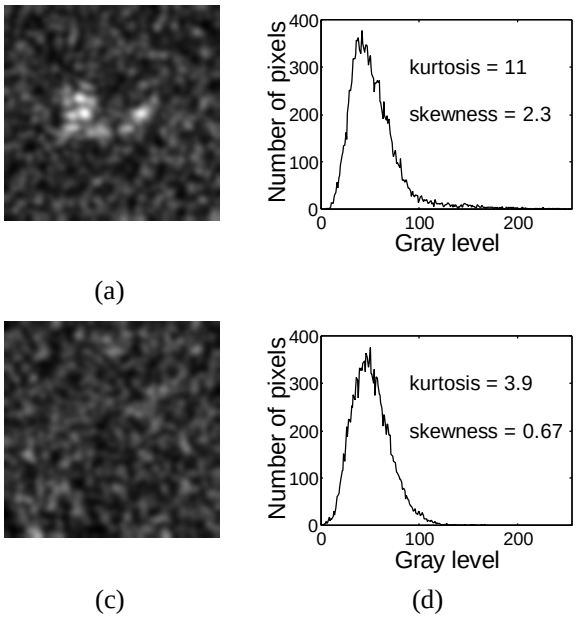

Figure 6. Modulus of the analytic channel responses and their corresponding histograms for two typical channels: (a) and (b), a channel well tuned to the moving object; (c) and (d), a channel equally tuned to the object and the background (also displayed skewness and kurtosis values).

2.2.2 *Selection of the best feature channels*

As we have just seen, descriptors obtained from the modulus (square root of the energy) of the channel responses can be used to discriminate between regions having different textures and/or motions. Each spatio-temporal location in the sequence is then characterized by a set of 10 (orientations) x 3 (scales) = 30 descriptors, which are the responses of the channels that are sampling the local spectrum. The number of components of this feature vector (30) is too high, making the computational cost of segmentation almost unaffordable. Moreover, as shown in Fig. 5, many of the channels will not contribute to discriminate object from background, but can even increase the segmentation errors (in particular for channels dominated by noise). Therefore, we have included an additional step, consisting of selecting a reduced number of (four) channels providing maximum discrimination. This selection improves the segmentation and strongly reduces the computational cost.

The method to select of the most representative channels relies on the characteristic features of our input sequences, which contain a moving object against a larger background either static or undergoing a different motion. As shown in Figure 6, the statistics of the channel responses can provide useful information for selecting them. This Figure compares the modulus of 2 of the 10 channels corresponding to the finest scale, for a frame of the test sequence of Figure 3. One channel (Figure 6a) is well tuned to the target motion, and therefore displays higher values (brighter gray levels) in the region occupied by it. Conversely, it tends to show lower responses (darker gray levels) in the background region, and therefore, this channel can be useful to discriminate between object and background. Interestingly, this discrimination capability is reflected in its histogram, which displays (Figure 6b): (1) a big lobe near the origin, corresponding to pixels in the background; and (2) a long tail extending towards higher values, which accounts for the strong responses given by the (fewer) pixels belonging to the object. Channels dominated by noise, and hence less appropriate to segment the sequence (Fig. 6c), display the big lobe near the origin (Fig. 6c), but not the long tail.

Therefore a good selection criterion is to pick those channels whose histograms display longer tails (i.e. contain some strong responses). This feature is appropriately characterized by conventional statistical normalized moments, like skewness or kurtosis. As shown in the example of Figure 6, both (skewness and kurtosis) are significantly higher (by a factor of nearly 3) for the upper discriminating channel than for the lower one (see values in Figure 6 b and d).

We have checked that both moments produced equally reasonable results in channel selection, for our test sequences, but we finally adopted kurtosis since it produced slightly better results. The number of selected channels is a trade-off between having as much information as possible, and a low computational cost. We found that those 4 channels (among the total of 30) having the highest kurtosis produced good segmentation results for our sequences at a reasonable low cost.

2.2.3 *Clustering*

The resulting feature vectors, composed by the modulus of the outputs of the 4 selected channels, are used to segment the sequence into 2 classes (object and background), using the standard k-means clustering algorithm[28]. We found that it is convenient to normalize the modulus of every channel independently, between 0 and 1, so that the selected channels enter with equal weight in the clustering process.

The clustering is performed frame by frame because the velocity of the translating object can change slowly in time. This strategy permits to initialize the clustering algorithm with the cluster centers found in the previous frame, which are very likely to be close to the present centers, thus reducing the number of iterations significantly for most frames. Finally, the segmentation results are refined by spatial median filtering (window size 11x11) each segmented frame, which removes possible small isolated regions with a high probability of corresponding to segmentation errors.

Results of segmentation for the synthetic test sequence (Fig. 3) are presented in Figure 7. Both the original (a) and

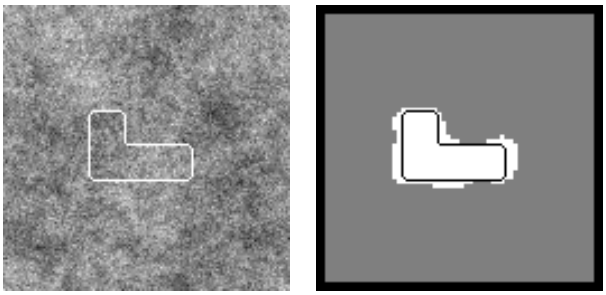

(a) (b)

Figure 7. Segmentation results for the synthetic test sequence: (a) original frame; (b) results of segmentation with 2 classes. The edge of the true object is overlaid in both images.

segmented (b) frames include the true border, overlaid on them to facilitate the visual localization of the target. Gray pixels in the segmented image have been assigned to the background, and the white pixels to the object. The target has been successfully segmented from the background by our fully automatic method. There are only some segmentation errors concentrated along the boundaries of the object, because the finite spatial support of the filters is mixing information from object and background. The average percentage of pixels correctly segmented was 98% for an ensemble of synthetic test sequences with different levels of noise, and velocities of the object and the background, which is a highly satisfactory result.

2.3 *Velocity estimation*

After segmenting the target, the next step consists of estimating its displacement between consecutive frames, which is necessary to register the object in all frames. For this purpose we estimate the velocity of the pixels inside the region occupied by the object, using an optical flow estimation algorithm[13]. Although there are other simpler techniques, like estimating the displacements of the segmented area through correlation, matching, etc., they are less robust, since segmentation results may be too noisy (particularly in real sequences with very low SNR) to estimate accurately the displacements of the segmented target. In our case, the optical flow estimation is performed by a specially adapted version of a probabilistic multichannel method[29,13], which is based on the visual representation of the sequence already obtained (see Section 2.1), thus requiring little additional cost. This step is performed frame by frame, and it produces a robust and accurate estimation of the translation velocity of the object (and of its associated covariance matrix) for each frame.

The optical flow algorithm is based on the classical gradient constraint[20], which is obtained under the assumption that intensity levels in the sequence can move their position but remain constant over time, so that the differential of the image with respect to time is zero. In traditional methods, the gradient constraint is set up at each spatio-temporal location (x, y, t) as follows:

$$s_x v_x + s_y v_y + s_t = 0 \tag{5}$$

where (s_x, s_y, s_t) is the spatio-temporal gradient of the input sequence s, and (v_x, v_y) is the 2D velocity vector. However, differentiating discrete sequences is numerically unstable and requires some regularization, like pre-filtering with a low-pass filter, to obtain good results. Since both filtering and deriving are linear operations, it turns out that it is equivalent to pre-filtering and then deriving than filtering directly with the derivative of the pre-filter. If the regularizing pre-filter is chosen to be a Gaussian filter, then spatio-temporal gradients are obtained filtering the sequence with the appropriate Gaussian derivative filters. Therefore, in our case the subscript associated to the input sequence s means that the sequence is filtered with the corresponding Gaussian derivative filter.

In the original multichannel method[13], the gradient constraint is applied to the output of a set of directional second order Gaussian derivative (GD2) filters. This strategy increases robustness since the gradient constraint is applied to the meaningful events in the sequence extracted by the GD2 filters, such as bars, edges or texture.Equation 5 takes then the specific form:

$$s_{h_0 h_0 x} v_x + s_{h_0 h_0 y} v_y + s_{h_0 h_0 t} = 0 \tag{6}$$

where $\vec{h}_0$ is the direction vector along which the second derivative is taken. This unique constraint does not permit one to solve for the two components of the image velocity (v_x, v_y) at each point, and thus different methods have been proposed to obtain additional constraints (equations) to solve for the 2D velocity. In our case, the object has been previously segmented and, according to the assumption of pure translation, all pixels in the object share the same velocity. Thus, it is possible to combine all their corresponding constraints, which gives the following overdetermined linear system:

$$\mathbf{Av} = \mathbf{b}, \quad \text{with}$$
$$\mathbf{A} = \begin{pmatrix} s^0_{h_0 h_0 x} & s^0_{h_0 h_0 y} \\ s^1_{h_0 h_0 x} & s^1_{h_0 h_0 y} \\ \vdots & \vdots \\ s^{N-1}_{h_0 h_0 x} & s^{N-1}_{h_0 h_0 y} \end{pmatrix}, \mathbf{v} = \begin{pmatrix} v_x \\ v_y \end{pmatrix}, \mathbf{b} = -\begin{pmatrix} s^0_{h_0 h_0 t} \\ s^1_{h_0 h_0 t} \\ \vdots \\ s^{N-1}_{h_0 h_0 t} \end{pmatrix} \tag{7}$$

where the super-index covers all the N points previously assigned to the target by the automatic segmentation. We solve this system using least-squares, which gives an estimate of the velocity $(\tilde{\mathbf{v}})$ and of its associated covariance matrix $(\mathbf{C}_\mathbf{v})$:

$$\tilde{\mathbf{v}} = \begin{pmatrix} \tilde{v}_x \\ \tilde{v}_y \end{pmatrix} = (\mathbf{A}^T\mathbf{A})^{-1}\mathbf{A}^T\mathbf{b} \quad (8)$$

$$\mathbf{C}_\mathbf{v} = (\mathbf{A}^T\mathbf{A})^{-1}\frac{1}{N-1}\sum_{i=0}^{N-1}(s^i_{h_0h_0x}\tilde{v}_x + s^i_{h_0h_0y}\tilde{v}_y + s^i_{h_0h_0t})^2 \quad (9)$$

Covariance matrices are important since they are 2D confidence measures of the velocity estimates, which are very useful to combine estimates from different sources[13], (spatio-temporal locations[30,31] channels, etc.).

The system in Eq. 7 may be set up for different directional GD2 channels, obtaining different estimates that can be combined to obtain a unique less noisy estimate (as is done in the original method[13]). In this particular application, we use only one GD2 channel, which is chosen to be tuned to the target motion (i.e., the GD2 channel with the strongest response to the object). Estimating the velocity at the output of a directional channel tends to increase the aperture problem, because the range of orientations is limited at the output of the filter. However, this effect is not too severe in our case for two reasons: 1) the GD2 filters are not very selective in orientation; and 2) there is a relatively large number of points from which the gradient constraint is combined, making highly likely the presence of different orientations, and thus diminishing the aperture problem. On the other hand, the great advantage of using a directional channel tuned to the object is that a high amount of noise is eliminated before estimating the velocity, and it also helps to minimize the influence of the background velocity (which can be important in pixels near the border of the target).

The channel selected for the velocity estimation is placed on the dynamic plane, given by $j = \text{asin}(5/8)$ in the frequency domain, so that only the azimuth is tuned to obtain maximum energy response to the object. This is achieved by evaluating the channel energy response as a function of the azimuth of the center frequency, and finding the azimuth of the channel giving maximum response. This function can be represented as a curve that can be easily obtained, since the energy response of derivative channels placed at arbitrary values of azimuth (directions in general) can be theoretically interpolated from the responses of a reduced set of channels because derivative filters are steerable[24]. The responses of 5 GD3 channels in the dynamic plane are available (Section 2.1), from which it is possible to obtain 5 energy measurements corresponding to the object (averaging the modulus of the response to the analytic channels across all pixels in the region corresponding to the object). In theory, we would need more than 9 measurements to obtain an accurate approximation of the interpolation[24], but we found that using the 5 available measurements produces good results for all tested sequences. Furthermore, the precision required in azimuth tuning is not critical for this application.

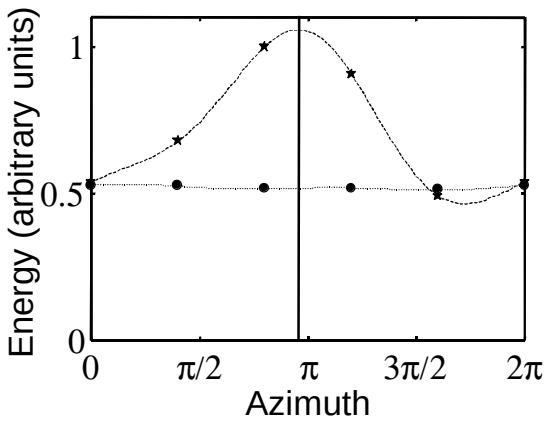

Figure 8. Interpolation of the 5 energy measurements for the regions segmented as background (circles, dotted line) and as object (stars, dashed line) as a function of the azimuth, for the test sequence in Figure 3. The azimuth corresponding to the true maximum for the object velocity of (4/3, -1/5) cycles/pixel is shown as a vertical line.

The graph in Figure 8 shows the results of interpolation for the same test sequence used previously. The five average energy measurements are marked with stars and circles for the object and the background, respectively. The interpolation curves are obtained applying theoretical interpolation functions for the case of having 5 harmonics (see Appendix F in Ref. [24]). The background curve (dashed) is almost constant, and is below the target's one. Since in this case the background is static, there is no preferred direction, and motion energy is only due to noise. The curve corresponding to the target (dotted) shows a clear maximum close to the theoretical azimuth (marked by the vertical line) corresponding to the direction of the object velocity, (4/3, -1/5) pixels/frame (known in this synthetic sequence).

It is important to note that there is no need to compute explicitly the response to the directional GD2 channels, since the spatio-temporal gradient of such GD2 channels $(s_{h_0h_0x}, s_{h_0h_0y}, s_{h_0h_0t})$ is easily obtained from the representation using the separable basis of GD3 (i.e., from the sequence filtered with all the partial GD3 derivatives) through the following linear combinations[13]:

$$s_{h_0h_0x} = h_{0_x}^2 s_{xxx} + h_{0_y}^2 s_{xxy} + h_{0_t}^2 s_{ttx} + 2h_{0_x}h_{0_y}s_{xxy} + 2h_{0_x}h_{0_t}s_{xxt} + 2h_{0_y}h_{0_t}s_{xyt} \quad (10)$$

$$s_{h_0h_0y} = h_{0_x}^2 s_{xxy} + h_{0_y}^2 s_{yyy} + h_{0_t}^2 s_{tty} + 2h_{0_x}h_{0_y}s_{yyx} + 2h_{0_x}h_{0_t}s_{xyt} + 2h_{0_y}h_{0_t}s_{yyt} \quad (11)$$

$$s_{h_0h_0t} = h_{0_x}^2 s_{xxt} + h_{0_y}^2 s_{yyt} + h_{0_t}^2 s_{ttt} + 2h_{0_x}h_{0_y}s_{xyt} + 2h_{0_x}h_{0_t}s_{ttx} + 2h_{0_y}h_{0_t}s_{tty} \quad (12)$$

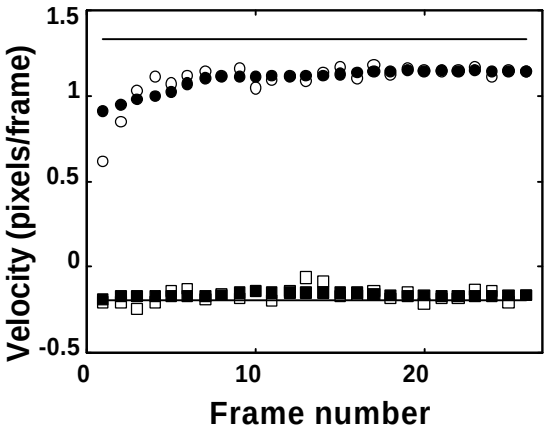

Figure 9. Estimates of the horizontal (circles) and vertical (squares) velocity for every frame of the test sequence, before (open symbols) and after (solid symbols) the combination in a temporal window of 9 frames. Also shown in continuous lines the real horizontal and vertical velocities of (4/3, -1/5) cycles/pixel.

where $(h_{0_x}, h_{0_y}, h_{0_t})$ are the components of the directional vector $\vec{h}_0$, given that its modulus is one ($\left|\vec{h}_0\right| = 1$).

2.4 *Registration and integration*

The last step is the registration of the moving object and the integration of all registered frames to increase the SNR. Registration can be achieved using the velocities, estimated in the previous stage, frame by frame. However, a further refinement of the velocity estimates of each frame is possible, by taking advantage of the assumption that the velocity of the object does not have large variations along the sequence. One simple strategy would be averaging the velocity estimates within a temporal window, but a more intelligent combination of velocities is possible taking into account the covariance matrices, which will produce a more robust and accurate estimate[13,29,30,31]. The combination of a set of estimates of the velocity from N consecutive frames, $\mathbf{v}_i = \left\{(\tilde{v}_{x_i}, \tilde{v}_{y_i})\right\}$, taking into account their associated covariance matrices $(\mathbf{C}_{\mathbf{v}_i})$, results in the following new estimate for the velocity (assuming that the different estimates are uncorrelated):

$$\tilde{\mathbf{v}} = \left(\sum_{i=0}^{N-1} \mathbf{C}_{\mathbf{v}_i}^{-1} \right)^{-1} \begin{pmatrix} \sum_{i=0}^{N-1} \dfrac{\tilde{v}_{x_i}}{s_{u_i}^2} + \dfrac{\tilde{v}_{y_i}}{s_{uv_i}} \\ \sum_{i=0}^{N-1} \dfrac{\tilde{v}_{x_i}}{s_{uv_i}} + \dfrac{\tilde{v}_{y_i}}{s_{v_i}^2} \end{pmatrix} \tag{13}$$

where $s_{u_i}^2$, s_{uv_i} and $s_{v_i}^2$ are the components of the covariance matrix:

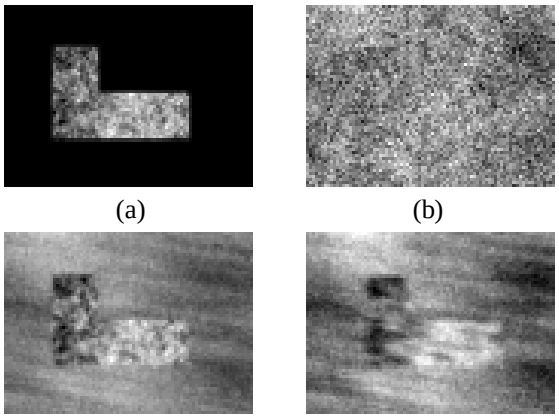

Figure 10. Results after the integration step for the test sequence: (a) original moving object; (b) noisy frame; (c) integration using the real velocity to register the object; (d) integration using the estimated velocities.

$$\mathbf{C}_{\mathbf{v}_i} = \begin{pmatrix} s_{u_i}^2 & s_{uv_i} \\ s_{uv_i} & s_{v_i}^2 \end{pmatrix} \tag{14}$$

The graph in Figure 9 displays the horizontal (circles) and vertical (squares) estimates of the velocity as a function of frame number, before (open symbols) and after (filled symbols) the temporal combination, for a synthetic test sequence with 0dB of SNR. The actual velocity of the object is constant for all frames: (4/3, -1/5) pixels/frame, and these two components are represented as two continuous lines in the graph. The horizontal velocity component has been underestimated. This can be caused by a bias in the estimate as a result of the simplified noise model that assumes noise-free spatial gradients[29,13]. The velocity estimates are much more stable after the temporal combination, which eliminates much of the noise present in each single frame estimate.

Finally, the frames are motion compensated using bilinear backward interpolation, based on the displacements predicted by the velocities estimated in the previous step. Bilinear interpolation introduces a slight low-pass filtering effect, as can be appreciated in Figure 10. This Figure compares the original noise-free object (a), the object in one of the noisy frames (b), and the result of integrating the 26 central frames using the actual velocity (c), and using the velocity estimates provided by our method (d). Even if we use the actual velocity there is some blurring effect due to the bilinear interpolation (compare images in Figure 10a and c). The result obtained applying all the steps of the automatic method (Fig. 10d) are satisfactory, the target appears clearly visible, although clearly blurred, mainly in the horizontal direction, as a result of the slight underestimation of that velocity component. Nevertheless, the shape and most of the texture of the original object appears clearly visible in the final result. It must be also con-

sidered that this test case corresponds to a very extreme situation with SNR=0dB (see Fig. 10b).

3 Results

We have applied this method to real sequences of ships recorded with static ground-mounted cameras for maritime surveillance. The sequences were taken using either an infrared camera operating on the 8-12 μm range, or a conventional CCD camera operating in the visible range. These sequences were severely affected by noise introduced by the system, but mainly by bad atmospheric conditions. In these sequences, the observed ship is translating without appreciable rotation or scaling, therefore satisfying the assumptions of the method. We present here results from two visible and one infrared sequences. The enhanced images are compared to one of the original frames.

The first sequence is 100 frames long and was taken with a visible camera. The ship is translating from right to the left, with a mean horizontal velocity of about 1 pixel/frame (estimated manually as an average velocity from the global displacement between first and last frames). Figure 11a plots the estimates of the horizontal and vertical velocity components at each frame, being approximately constant and equal to the mean velocity estimated manually. Fig. 11b displays one of the original frames, where most details of the ship are lost or masked by noise. The result, after applying our fully automatic method, is shown in Fig. 11c. The image has been strongly enhanced, the target displays now many details that were not visible in the original frame and the SNR is much higher. There is again a blurring effect that comes from both the bilinear interpolation and errors in the displacement estimation.

An original frame of the second visible sequence, 50 frames long, is shown in Figure 12b. The ship is translating from right to the left with an average horizontal velocity of about 0.7 pixels/frame (estimated manually). The horizontal estimated velocities in the graph of Figure 12a oscillate around this average value, between 0.5 and 1 pixel/frame. The vertical velocity component is approximately equal to zero. The noise level is similar here than in the previous sequence, making difficult the recognition of details, especially on the right side of the ship. These details are clearly visible, however, in the final enhanced image, Fig. 12c. In addition, the hull of the ship appears more uniform almost noise-free.

The last example corresponds to a sequence 25 frames long, taken with the infrared camera, where the ship is translating from left to the right at an average horizontal velocity of 0.9 pixels/frame. The estimated velocities are close to this average value, as shown in the graph in Figure 13a. An original frame and the resulting enhanced image, both in inverse video (hot areas darker), are also shown in Figs. 13b and 13c respectively. The original frame is slightly less noisy than the visible case since atmospheric conditions affect less to infrared images., Nevertheless, there is again a great improvement in the resulting image. Four vertical bars that seem to be funnels, which were hardly visible in the original image (Fig. 13b), appear clear in the enhanced image (Fig. 13c).

4 Conclusions

We have developed a fully automatic method that produces an enhanced image of an object from a very noisy sequence, where the object is subject to a smooth translation motion. This is achieved by the well-known technique of averaging several frames to reduce the random noise, but since the object is moving it is necessary to estimate and compensate motion before averaging. This task is not trivial, even when the object is simply translating, due to the high level of noise, which makes the application of conventional techniques to estimate the displacements impractical.

An optimal solution is the simultaneous estimation and segmentation of the image velocity, using algorithms like Expectation/Maximization (E/M)[11]. This solution is applicable to general models of image sequences including translation, rotation and scaling. Indeed, these methods have proven very useful in noise-free images. However, they are usually very costly, they have critical parameters that have to be finely tuned, the convergence rate is usually relatively slow, and the final result depends critically on the initial condition. Given the high amount of noise present in our sequences, we have taken advantage of the simple translation model of the sequences to apply a more efficient and robust technique. Therefore, we segment the pixels based on the local spatio-temporal spectrum as a reliable description of the local texture-motion content, which is possible due to the simple translational model of sequences of interest. The clustering is then performed using a simple clustering algorithm (k-means). The results obtained in segmentation of synthetic test sequences, with different amounts of noise, and different translation velocities of the object and the background, confirm the robustness of this strategy (mean percent of correct segmented pixels greater then 98%).

The velocity of the target can then be estimated robustly, since the segmentation process has grouped together all the pixels sharing the same motion. Other segmentation strategies not based in motion (e.g., based on the intensity level, etc.) will produce poor results due to noise, and can group together pixels having different motion, thus spoiling the robust estimation of the velocity. Additional robustness is achieved by estimating the optical flow at the output of a directional band-pass filter, in the spatio-temporal frequency domain, tuned to the moving object, which therefore minimizes the effect of noise as well as the potential contamination by responses due to the background in the occlusion boundaries.

(a) (b) (c)

Figure 11. Results for the first real sequence of a ship taken from a static CCD camera within the range of visible: (a) plot of the horizontal (dashed line) and vertical (dotted line) velocities of the object at each frame; (b) subregion of original middle frame; (c) final enhanced image.

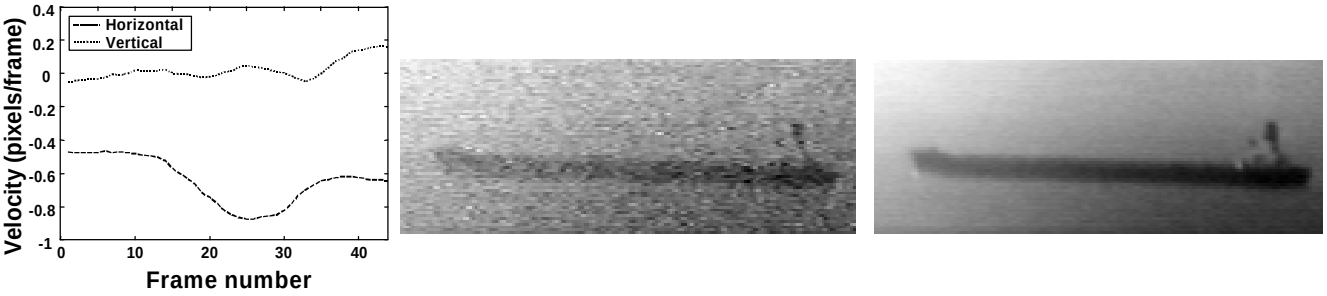

(a) (b) (c)

Figure 12. Results for the second real sequence of a ship taken from a static CCD camera within the range of visible: (a) plot of the horizontal (dashed line) and vertical (dotted line) velocities of the object at each frame; (b) subregion original middle frame; (c) final enhanced image.

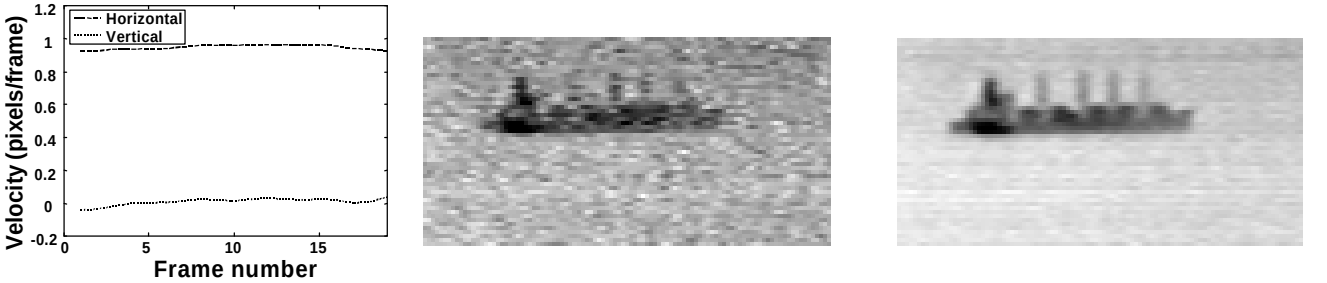

(a) (b) (c)

Figure 13. Results in a real sequence of a ship taken from a infrared imaging system within the range of 8-12 μm: (a) plot of the horizontal (dashed line) and vertical (dotted line) velocities of the object at each frame; (b) subregion original middle frame; (c) final enhanced image.

The velocity estimates are then used to register the object along all the frames. Once the target is registered, all the frames are averaged to reduce the noise, producing an enhanced image of the object. The excellent results obtained in real sequences from maritime surveillance systems (both visible and infrared) demonstrate the validity of the approach, and the usefulness of the method.

Acknowledgements

This research has been supported by the Comisión Interministerial de Ciencia y Tecnología of Spain, grant TIC98-0925-C02-01. We whish to thank David Fleet (Xerox PARC) for revising the final version of the manuscript.

References

1. B. Cohen, V. Avrin, M. Belitsky, and I. Dinstein, "Generation of a restored image from a video sequence recorded under turbulence effects", *Opt. Eng.*, **36**(12), 3312-3317 (1997).
2. W. K. Pratt, *Digital Image Processing*, Wiley-Interscience, New York, (1991).
3. J. C. Russ, *The Image Processing Handbook*, CRC Press, Boca Raton (1995).
4. R. C. Hardie, K. J. Barnard, J. G. Bognar, E. E. Armstrong, and E. A. Watson, "High-resolution image reconstruction from a sequence of rotated and translated frames and its application to an infrared imaging system", *Opt. Eng.*, **37**(1), 247-260 (1998).
5. M. S. Alam, J. G. Bognar, S. Cain, and B. Yasuda, "Fast registration and reconstruction of aliased frames by use of a modified maximum-likelihood approach", *Applied Optics*, **37**(8), 1319-1328 (1998).
6. D. Granrath and J. Lersch, "Fusion of images on affine sampling grids", *J. Opt. Soc. Am. A*, **15**(4), 791-801 (1998).
7. M. Bertero, T. Poggio, and V. Torre, "Ill-posed problems in early vision", *Proceedings of the IEEE*, **76**, 869-889 (1988).
8. J. Barron, D. Fleet, S. Beauchemin, and T. Burkitt, "Performance of optical flow techniques", *International Journal of Computer Vision*, **12**, 43-77 (1994).
9. Y. Weiss and E. H. Adelson, "Representing moving images with layers", *IEEE Trans. on Image Processing*, **3**(5), 625-638 (1994).
10. J. Shi and J. Malik, "Motion segmentation and tracking using normalized cuts", *in International Conference on Computer Vision* (1998).
11. Y. Weiss and E. H. Adelson, "A unified mixture framework for motion segmentation: incorporating spatial coherence and estimating the number of models", *in Proc. IEEE Conf. Comput. Vision Pattern Recog.*, 321-326 (1996).
12. M. Shizawa and K. Mase, "Simultaneous Multiple Optical Flow Estimation", *in Proc. of the IEEE International Conference on Image Processing*, 274-278 (1990).
13. O. Nestares and R. Navarro, "Probabilistic Multichannel Optical Flow Analysis, Based on a Multipurpose Visual Representation of Image Sequences", *in Proc. of the SPIE*, **3644**, 429-440 (1999).
14. O. Nestares, C. Miravet, J. Santamaria, and R. Navarro, "Automatic Segmentation of Low Visibility Moving Objects through Energy Analysis of the Local 3D Spectrum", *in Proc. of the SPIE*, **3642**, 13-22 (1999).
15. E. H. Adelson and J. R. Bergen, "Spatiotemporal energy models for the perception of motion", *J. Opt. Soc. Am. A*, **2**(2), 284-299 (1985).
16. H. Knutsson, and G. H. Granlund, "Texture analysis using two-dimensional quadrature filters", *IEEE Workshop on Computer Architecture for Pattern Analysis and Image Data Base Management*, (1983).
17. M. Unser, "Multichannel static texture segmentation", *Signal Processing*, **11**, 61-79 (1986).
18. A. K. Jain and F. Farrokhnia, "Unsupervised texture segmentation using Gabor filters", *Pattern Recognition*, **24**(12), 1167-1186 (1991).
19. O. Nestares, R. Navarro, J. Portilla, and A. Tabernero, "Automatic computation of the area irradiated by ultrashort laser pulses in Sb materials through texture segmentation of TEM images", *Ultramicroscopy*, **66**(1-2), 101-115 (1996).
20. B. K. Horn and B. G. Schunk, "Determining optical flow", *Artificial Intelligence*, **17**, 185-203 (1981).
21. R. A. Young and R. M. Lesperance, "A physiological model of motion analysis for machine vision", *in Proc. of the SPIE*, **1913** (1993).
22. E. P. Simoncelli and D. J. Heeger, "A model of neuronal responses in visual area MT", *Vision Research*, **38**, 743-761 (1998).
23. C. H. Edwards, *Advanced calculus of several variables*, Dover Publications, Inc., New York (1973).
24. W. T. Freeman and E. H. Adelson, "The design and use of steerable filters", *IEEE Trans. on Patt. Anal. and Machine Intell.*, **13**(9), 891-906 (1991).
25. A. B. Watson and A. J. Ahumada, "Model of human visual-motion sensing", *J. Opt. Soc. Am. A*, **2**(2), 322-342 (1985).
26. M. Unser and M. Eden, "Nonlinear operators for improving texture segmentation based on features extracted by spatial filtering", *IEEE Trans. On Systems, Man, and Cybernetics*, **20**, 804-815 (1990).
27. T. Aach, A. Kaup, and R. Mester, "On Texture Analysis: Local Energy Transforms versus Quadrature Filters", *Signal Processing*, **45(**2), 173-181 (1995).
28. H. Nyblack, *Digital Image Processing*, Prentice-Hall, Englewood Clifs (1986).
29. E. P. Simoncelli, E. H. Adelson, and D. J. Heeger, "Probability distributions of optical flow", ", *in Proc. IEEE Conf. Comput. Vision Pattern Recog.*, 310-315 (1991).

30. A. Singh, "Incremental Estimation of Image-Flow Using a Kalman Filter", *Journal of Visual Communications and Image Representation*, **3**, 39-57 (1992).
31. M. R. Luettgen, W. C. Karl, A. S. Willsky, "Efficient multiscale regularization with applications to the computation of optical flow", *IEEE Trans. On Image Processing*, **3**(1), 41-64 (1994).

Oscar Nestares graduated in Electrical Engineering in 1994 from Universidad Politécnica de Madrid (Spain). He has worked on image and sequence processing at the Image and Vision group of the Instituto de Optica, Consejo Superior de Investigaciones Científicas from 1992 to 1997, when he received his PhD degree from Universidad Politécnica de Madrid. During 1998 he worked as a R&D Engineer in the Electro-optics section of the Aerospace Division of SENER Ingeniería y Sistemas S.A. He is currently a postdoctoral student (under the Fulbright Program) in the Department of Psychology of the Stanford University. He is interested in human and computer vision, computer models of the human visual system and image sequences processing.

Carlos Miravet received his MS in Physics from Madrid Complutense University in 1986. Since then, he has hold posts in national and international industrial and research and development institutions related to the fields of Electro-optics and image processing. Currently he is a senior engineer in the Electro-optics section of the Aerospace Division of SENER Ingeniería y Sistemas S.A.

Javier Santamaría received his MS and PhD degrees in physics from the University of Zaragoza, Spain, in 1969 and 1973 respectively. In 1972 he joined the Instituto de Optica, Madrid, where he was working as a research scientist in the fields of image evaluation, image processing and vision. He has been head of the Imaging and Vision Department until 1988 when he began to work at SENER Aerospace Division where he is responsible for the Electro-optics group. He has been regularly publishing scientific papers and presenting communications to international meetings. He was president of the Spanish Optical Society (1990-92) and member of the Advisory Committee of the European Optical Society (1993-96) His current research interest include Electro-optical system performance, automatic target recognition and image enhancement and restoration.

Rafael Navarro received the MS and PhD degrees in physics from theUniversity of Zaragoza, Spain, in 1979 and 1984 respectively. From 1985 to 1986 he was an optical and image processing engineer at the Instituto de Astrofísica de Canarias. Since 1987 he is a senior scientific researcher at the Instituto de Óptica, Consejo Superior de Investigaciones Científicas, where he has headed the Imaging & Vision group since 1988, and currently is associate director. He has been visiting researcher at the University of Rochester and at the U.C. Berkeley. He is member of the OSA, EOS, IEEE Signal Processing and ARVO, and his research interests are physiological optics, vision and image processing.